npj | quantum information

Article

Published in partnership with The University of New South Wales

https://doi.org/10.1038/s41534-025-01163-1

Distributed photonic variational quantum eigensolver with parameterized weak measurements

Donghwa Lee[1], Bohdan Bilash[1,2], Jaehak Lee[1,2], Hyang-Tag Lim[1,2], Yosep Kim[1,3], Seung-Woo Lee[1,4] & Yong-Su Kim[1,2] ✉

We demonstrate a two-qubit variational quantum eigensolver (VQE) implementation using two spatially separated single-photon processors connected via a 3 km optical fiber network. Our approach leverages local operations on pre-shared entanglement to evaluate two-qubit Hamiltonians. By incorporating parameterized weak measurement operations within the local operations framework, we enable access to the complete Hilbert space across distributed quantum processors – a capability typically requiring complex non-local operations. Our experimental results show accurate ground state energy estimation for Hamiltonians including H-He^+ cation and the Schwinger model, validating both the necessity of weak measurements and high-quality entanglement in distributed quantum computing. This work establishes a promising direction for resource-efficient, scalable quantum network architectures that maintain full computational capabilities through local operations and controlled entanglement manipulation.

Implementing large-scale quantum systems presents a major challenge, requiring scalable architectures that ensure high-fidelity state preparation and operations[1,2]. One promising approach is distributed quantum computing (DQC), where small, well-controlled qubit modules are interconnected via pre-shared entangled states, known as network qubits[3–6]. Within each module, circuit qubits execute local quantum operations, while network qubits mediate inter-module interactions, enabling cooperative large-scale quantum computation. To fully exploit the computational space of distributed circuit qubits, pre-shared entanglements across network qubits is essential for facilitating inter-module connectivity control.

In traditional DQC approaches, non-local operations based on quantum gate teleportation allow the implementation of a universal gate set across the network[7–10]. However, these methods typically require complicated protocols involving multiple gates, additional ancilla qubits, and classical communication, which can introduce errors and reduce fidelity as the system scales. This raises the question: can we simplify the distributed quantum computing paradigm while maintaining access to the full computational Hilbert space?

Weak measurement offers a promising alternative for controlling entanglement in distributed quantum systems[11–13]. Unlike projective measurements that collapse quantum states entirely, weak measurements induce partial collapses, allowing for the tuning of entanglement between distant qubits. By controlling the measurement strength, one can access quantum states that would otherwise require non-local operations.

In this paper, we demonstrate the feasibility of distributed quantum computing by employing parameterized weak measurement. Using a basic configuration in which two modules each host a network qubit, we show that the non-local operations traditionally required for establishing arbitrary entangled states can be effectively replaced by local operations combined with weak measurement. Specifically, we prove that this approach enables the preparation of any arbitrary two-qubit state, thus accessing the full Hilbert space necessary for quantum algorithms. We integrate this technique into a variational quantum eigensolver (VQE) framework[14–16], which relies on parameterized quantum state preparation and measurement, validating that high-fidelity quantum computations remain achievable in distributed architectures. Our experimental implementation using photonic qubits demonstrates that weak measurement can serve as a practical tool for entanglement manipulation in networked quantum processors, potentially simplifying the requirements for scaling up quantum computing resources.

Results

Variational quantum eigensolver

The variational quantum eigensolver (VQE) is a hybrid quantum-classical algorithm designed to find the ground state energy of a quantum system

[1]Center for Quantum Technology, Korea Institute of Science and Technology (KIST), Seoul, Republic of Korea. [2]Division of Quantum Information, KIST School, Korea University of Science and Technology, Seoul, Republic of Korea. [3]Department of Physics, Korea University, Seoul, Republic of Korea. [4] Department of Physics, Pohang University of Technology (POSTECH)P, Pohang, Republic of Korea. ✉e-mail: yong-su.kim@kist.re.kr

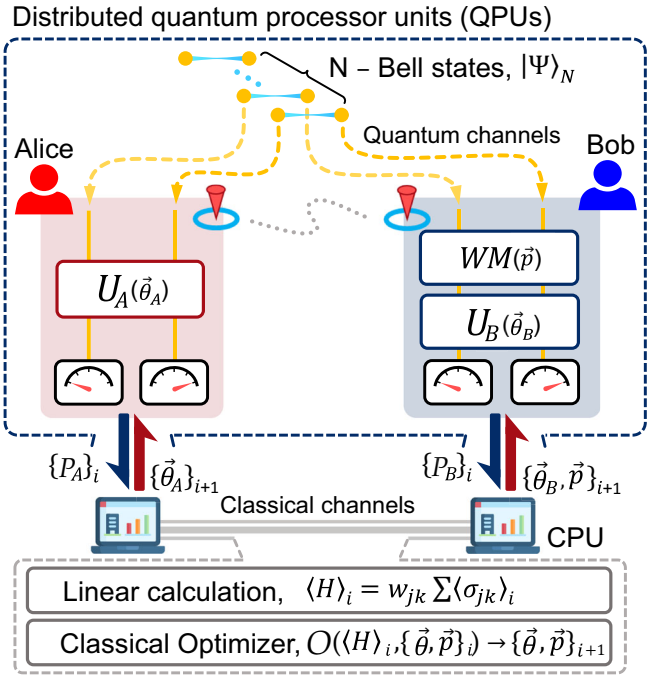

Fig. 1 | Schematic diagram of distributed VQE. Two spatially separated QPUs share N pairs of Bell states, with Alice performing local unitary operations $U_A(\vec{\theta}_A)$ and Bob implementing both local unitaries $U_B(\vec{\theta}_B)$ and weak measurements $WM(\vec{p})$. Measurement outcomes are sent to classical processing units (CPU) which computes the expectation value of the Hamiltonian and updates the parameters for subsequent iterations.

described by a Hamiltonian H[14–16]. VQE leverages the variational principle of quantum mechanics, which states that for any trial wavefunction $|\Psi(\vec{\theta})\rangle$, the expectation value of the Hamiltonian provides an upper bound to the ground state energy:

$$E(\vec{\theta}) = \langle \Psi(\vec{\theta})|H|\Psi(\vec{\theta})\rangle \geq E_g, \tag{1}$$

where E_g is the true ground state energy, and $\vec{\theta}$ represents a set of variational parameters that characterize the trial wavefunction.

The VQE algorithm operates as follows: First, a parameterized quantum circuit prepares a trial state $|\Psi(\vec{\theta})\rangle$, commonly referred to as an ansatz state. To measure the expectation value of the Hamiltonian $E(\vec{\theta})$, the Hamiltonian is decomposed into a linear combination of Pauli strings:

$$H = \sum_i c_i P_i, \tag{2}$$

where c_i are real coefficients and P_i are tensor products of Pauli operators (e.g., $X \otimes Y \otimes Z$). This decomposition allows the expectation value to be calculated as a weighted sum of expectations of Pauli operators, $\langle H\rangle = \sum_i c_i\langle P_i\rangle$, which can be measured directly on the quantum hardware through appropriate basis rotations. A classical optimizer subsequently updates the parameters $\vec{\theta}$ to minimize this energy expectation value:

$$E_g = \min_{\vec{\theta}}[E(\vec{\theta})]. \tag{3}$$

This iterative process continues until the energy converges, at which point the algorithm has approximated the ground state energy and corresponding wavefunction of the system. The effectiveness of VQE depends on the expressibility of the ansatz, which determines the algorithm's ability to represent the true ground state within the parameterized family of states.

While VQE has been primarily implemented on single quantum processors with various physical platforms[17–24], the growing interest in quantum networks opens new possibilities for distributed quantum computing[25,26]. In a networked environment, quantum processors at different locations can collaborate to solve computational problems that might be intractable for individual nodes. This distributed approach to VQE requires careful consideration of how entanglement and quantum operations are managed across the network.

VQE on quantum network

Figure 1 presents the schematic diagram of VQE between distant parties. Let us begin by a central party distributes a Bell state $|\Psi^+\rangle = \frac{1}{\sqrt{2}}(|01\rangle + |10\rangle)$ to two distant parties, Alice and Bob, via quantum channels. Without loss of generality, we can present the shared state between Alice and Bob in the form of

$$|\Psi\rangle = (I_A \otimes C_B)|\Psi^+\rangle = \frac{1}{\sqrt{2}}(|0\rangle \otimes |\psi_b\rangle + |1\rangle \otimes |\psi_b^\perp\rangle), \tag{4}$$

where I_A and C_B are Alice's identity channel and Bob's arbitrary unitary channel which satisfies $C_B|1\rangle = |\psi_b\rangle$ and $C_B|0\rangle = |\psi_b^\perp\rangle$. Note that $|\psi_b\rangle$ and $|\psi_b^\perp\rangle$ are orthogonal, i.e., $\langle\psi_b|\psi_b^\perp\rangle = 0$. It is notable that Eq. (4) remains in a perfect entangled state since local unitary channels do not change the amount of entanglement[27]. This means that, with only local unitary operations, Alice and Bob cannot access the full Hilbert space to find the solution of a given Hamiltonian.

In order to adjust amount of entanglement of distributed states, we apply weak measurements or partial collapse measurements on Bob's qubit[11–13]. The weak measurements on an arbitrary state $|\psi_b\rangle$ can be represented as

$$\begin{aligned} M_0^{(\psi_b)} &= |\psi_b\rangle\langle\psi_b| + \sqrt{1-p}|\psi_b^\perp\rangle\langle\psi_b^\perp|, \\ M_1^{(\psi_b)} &= \sqrt{p}|\psi_b^\perp\rangle\langle\psi_b^\perp|, \end{aligned} \tag{5}$$

where $0 \leq p \leq 1$ represents the weak measurement strength. Note that while $M_1^{(\psi_b)}$ leads to a complete projection onto $|\psi_b^\perp\rangle$, $M_0^{(\psi_b)}$ produces only a partial collapse towards $|\psi_b\rangle$, thus called weak measurement.

Now, we apply this weak measurement operation $M_0^{(\psi_b)}$ to the pre-shared state, yielding the post-measurement state:

$$(I \otimes M_0^{(\psi_b)})|\Psi\rangle \propto \frac{1}{\sqrt{2}}(|0\rangle \otimes M_0^{(\psi_b)}|\psi_b\rangle + |1\rangle \otimes M_0^{(\psi_b)}|\psi_b^\perp\rangle), \tag{6}$$

and the normalized post-selected state becomes

$$|\Psi(p)\rangle = \frac{1}{\sqrt{2-p}}(|0\rangle \otimes |\psi_b\rangle + \sqrt{1-p}|1\rangle \otimes |\psi_b^\perp\rangle). \tag{7}$$

From Eq. (7), we can understand the role of weak measurement in the networked VQE as a tuning knob for the amount of entanglement. For example, when $p = 0$, the measurement has no effect, equivalent to a perfect transmission channel that preserves maximal entanglement. On the other hand, $p = 1$ corresponds to a complete projection onto $|\Psi(p=1)\rangle \rightarrow |0\rangle|\psi_b\rangle$, collapsing the entangled state into a fully separable state. Quantitatively, the concurrence of the output state in Eq. (7), which quantifies the amount of entanglement, is given as

$$\mathcal{C}(p) = \frac{2\sqrt{1-p}}{2-p}. \tag{8}$$

Then, Alice and Bob perform local unitary operations (U_A, U_B) to explore the minimum state energy. Together with Bob's weak measurement,

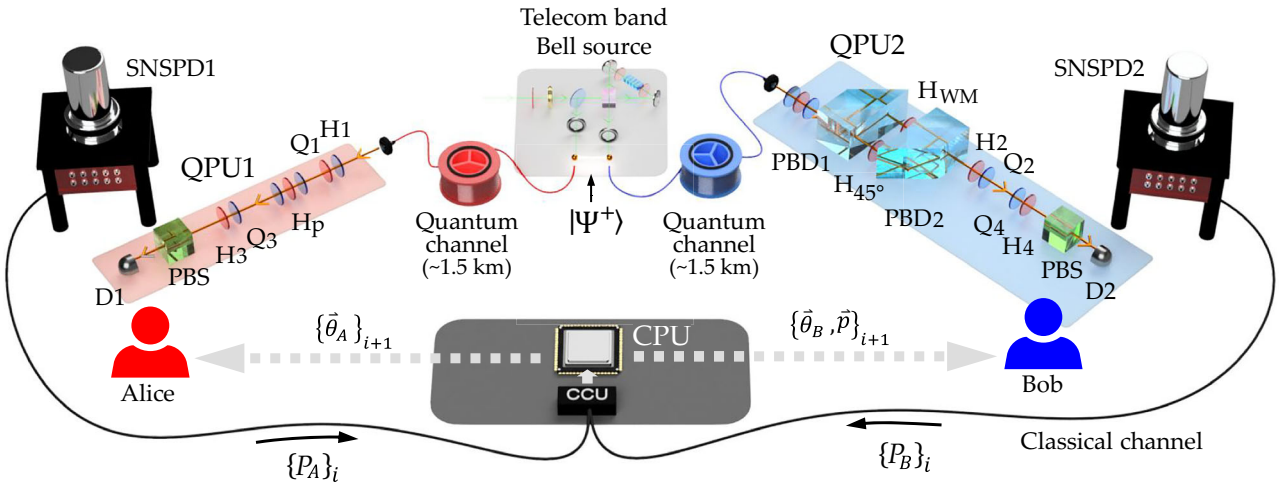

Fig. 2 | Experimental setup of the VQE on distributed quantum processors. The central source produces telecom-wavelength Bell states, which are distributed to Alice and Bob via 1.5 km optical fiber links. Each QPU contains waveplates (H, Q) for local operations, with Bob's QPU additionally incorporating a Mach-Zehnder interferometer with polarization beam displacers (PBDs) to implement weak measurements. Measurement results from superconducting nanowire single-photon detectors (SNSPDs) are collected by the central coincidence counting unit (CCU).

these local unitary operations enable them to explore entire space of pure two-qubit states. To prove this, let us rewrite Eq. (7) in the general Schmidt decomposition with a parameter θ where $\sqrt{1-p} = \tan\theta$[27]. Then Eq. (7) can be represented as

$$|\Psi(\theta)\rangle = \cos\theta|0\rangle \otimes |\psi_b\rangle + \sin\theta|1\rangle \otimes |\psi_b^{\perp}\rangle. \tag{9}$$

This explicitly takes the form of the Schmidt decomposition.

According to the Schmidt decomposition theorem, any arbitrary two-qubit pure state can be represented as:

$$|\phi\rangle = (U_A \otimes U_B)(\cos\theta|e_0\rangle \otimes |f_0\rangle + \sin\theta|e_1\rangle \otimes |f_1\rangle), \tag{10}$$

where $|e_0\rangle, |e_1\rangle$ and $|f_0\rangle, |f_1\rangle$ are orthonormal bases for the first and second qubits, respectively. Therefore, by applying appropriate local unitary operations to the state in Eq. (9), Alice and Bob can generate any arbitrary two-qubit pure state:

$$|\Psi_{\text{arb}}\rangle = (U_A \otimes U_B)|\Psi(\theta)\rangle, \tag{11}$$

where $\{|0\rangle, |1\rangle\} \xrightarrow{U_A} \{|e_0\rangle, |e_1\rangle\}$ and $\{|0\rangle, |1\rangle\} \xrightarrow{U_B} \{|f_0\rangle, |f_1\rangle\}$.

We can generalize our method to the d-dimensional case with $d = 2^n$. The resources required to explore the whole $d \times d$ Hilbert space are a maximally entangled two-qudit state and local operations and classical communication (LOCC)[28,29]. The maximally entangled state can easily be prepared with n pairs of Bell states, written as

$$|\Phi^+\rangle^{\otimes n} = \bigotimes_{m=0}^{n-1} \frac{1}{\sqrt{2}} \sum_{x_m=0}^{1} |x_m, x_m\rangle = \frac{1}{\sqrt{2^n}} \sum_{k=0}^{2^n-1} |k, k\rangle, \tag{12}$$

where $x_0 x_1 x_2 \cdots x_{n-1(2)}$ is a binary representation of k.

Starting from the maximally entangled state, it is possible to explore the whole $d \times d$ Hilbert space using LOCC transformation, provided that arbitrary local operations are available to both Alice and Bob. In general, implementing arbitrary operations on d qubits requires nonlinear two-qubit operations. In particular, a joint weak measurement on two qubits, represented as

$$M_0 = |00\rangle\langle 00| + |01\rangle\langle 01| + |10\rangle\langle 10| + \sqrt{1-p}|11\rangle\langle 11|, \tag{13}$$

$$M_1 = \sqrt{p}|11\rangle\langle 11|, \tag{14}$$

cannot be implemented simply by applying two separate weak measurements on each qubit individually. In such cases, we can expand the experimentally accessible Hilbert space by employing nonlocal measurements acting jointly on multiple qubits[30–34]. It would be interesting to explore optimization strategies within experimentally reliable nonlocal measurements. However, the goal of VQE is to find ground states of given Hamiltonians rather than prepare arbitrary quantum states. Investigating which classes of Hamiltonians admit ground states accessible through local weak measurements alone constitutes an important direction for future research.

Scaling to n Bell pairs distributed across the network, our approach maintains practical resource efficiency. The weak measurement strategy requires $\mathcal{O}(n)$ strength parameters-one per Bell pair-enabling tunable entanglement control across all network qubits. Combined with local unitary operations, this provides access to a wide range of 2^{2n}-dimensional Hilbert space needed for VQE. The total number of parameters remains polynomial: $\mathcal{O}(n)$ to $\mathcal{O}(n^2)$ for typical hardware-efficient ansatz and $\mathcal{O}(n)$ weak measurement parameters[16,18]. This avoids the complexity of gate teleportation, which requires additional Bell pairs and classical communication for each non-local gate, with overhead scaling with the circuit depth rather than just the system size. By leveraging pre-shared entanglement as a foundation and using weak measurements to tune entanglement levels, our approach provides a resource-efficient pathway for scaling quantum networks with multiple Bell pairs between nodes.

Experimental results

Figure 2 shows the experimental setup of the photonic VQE, which consists of pre-shared entanglement and two distant QPUs. At the center of the setup, a Sagnac interferometer with a periodically poled KTP crystal generates Bell states:

$$|\Psi^+\rangle = \frac{1}{\sqrt{2}}(|HV\rangle + |VH\rangle), \tag{15}$$

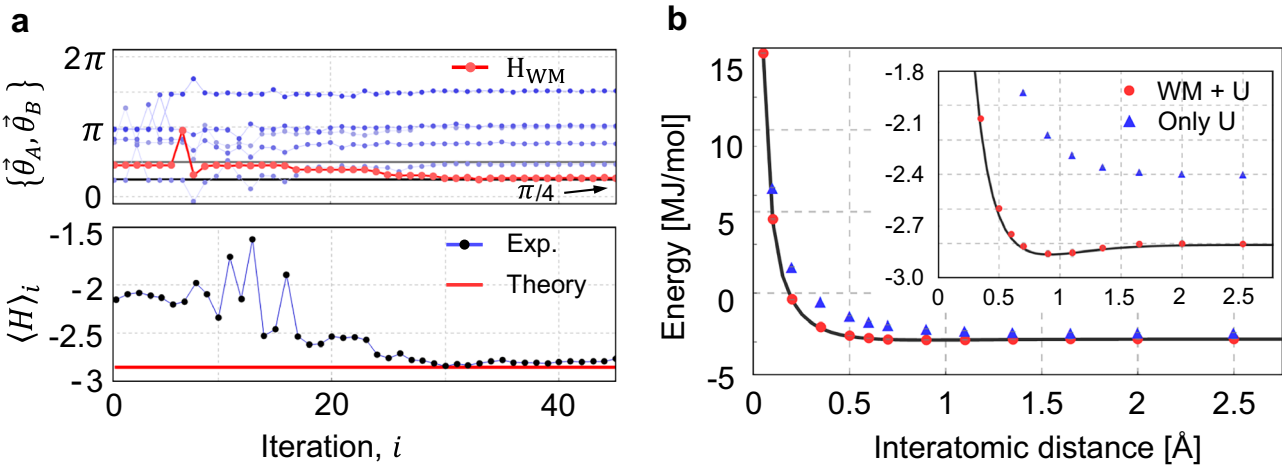

Fig. 3 | Experimental results for the evaluation of the H-He$^+$ cation using distributed quantum processors. a Convergence of the estimated energy and input parameters during a single VQE run at $R = 0.9$ Å. **b** Ground state energy as a function of interatomic distance, comparing results with and without weak measurement. Error bars are smaller than the size of markers.

where $|H\rangle$ and $|V\rangle$ represent horizontal and vertical polarization states, respectively, corresponding to the spin eigenstates $|0\rangle$ and $|1\rangle$[35–37]. It generates high quality Bell state with the purity and concurrence of $P = 0.98 \pm 0.01$, and $C = 0.98 \pm 0.01$, respectively.

Each single-photon state is then transmitted to Alice and Bob via two 1.5 km-long optical fibers. Upon receiving a single-photon, Alice's QPU applies an arbitrary local unitary transformation using a combination of a half-wave plate and a quarter-wave plate (H_1, Q_1). Additionally, she has a half waveplate H_P placed between two quarter waveplates at 45°, which modifies the relative phase between the two components of the initial Bell state of Eq. (15)[38]. Overall, Alice has three parameters $\vec{\theta}_A = \{H_1, Q_1, H_P\}$ for her ansatz state preparation via $U_A(\vec{\theta}_A)$. Following this, the Pauli basis measurements are performed by sets of waveplates (H3, Q3), a polarizing beamsplitter (PBS), and a single-photon detector (D1). The measurement results $\{P_A\}$ and $\vec{\theta}_A$ are sent to a classical process unit (CPU) located between Alice and Bob for further processing in the VQE loop.

Bob's QPU operates in a similar manner to Alice's, but with an additional weak measurement stage. Upon receiving a single-photon, Bob first implements the weak measurement using a Mach-Zehnder interferometer with two polarization beam displacers (PBDs) and two half-wave plates. The PBD transmits horizontal (vertical) polarization state without (with) lateral displacement. While one of the half waveplates is fixed at 45° ($H_{45°}$), the other's angle is controlled by an input parameter H_{WM}. This way, Bob can change the weak measurement strength p by adjusting the angle of H_{WM}. After the weak measurement, the local unitary operation and Pauli measurement are performed using a set of waveplates of H_2, Q_2 and H_4, Q_4, a PBS and a single-photon detector (D2). Overall, Bob's local operations can also be parametrized with three wavelplate angles of $\vec{\theta}_B = \{H_{WM}, H_2, Q_2\}$. The input parameters $\vec{\theta}_B$ with the Pauli measurement results $\{P_B\}$ are sent to the CPU in the middle as well.

After both QPUs complete their executions, a home-made coincidence counting unit (CCU) in the middle of Alice and Bob receives the joint Pauli measurement results[39,40]. With the six input parameters of $\{\vec{\theta}_A, \vec{\theta}_B\} = \{H_1, Q_1, H_P, H_{WM}, H_2, Q_2\}$ and the joint Pauli measurement results, the CPU performs linear calculation and classical optimization. In the linear calculation process, the CPU calculates the expectation value of Hamiltonian at the i-th VQE iteration $\langle H\rangle_i$ in Eq. (3). Then, with the six input parameters $\vec{\theta}_i$ and $\langle H\rangle_i$, the classical optimizer updates the next input parameters, $\vec{\theta}_{i+1}$, to find the minimum expectation value $\langle H\rangle_{\min}$ and transmits to Alice and Bob for the next VQE run. In our experiment, we employed the COBYLA algorithm to perform the classical optimization with *tol* = 0.01 and *rhobeg*=$\pi/2$[41], with a 200 max iteration cap that was typically sufficient for convergence and restarts otherwise[21]. See Methods for details. The experimental values and error bars are obtained by taking averages and standard deviations of the five lowest energy points during a single VQE run.

In order to verify our photonic VQE on two distributed QPUs, we estimated the ground state energy of the H-He$^+$ cation. The Hamiltonian of this simple cation is described by two Pauli operators, providing an ideal test case for our distributed VQE setup[14]. The detailed form of the Hamiltonian with respect to the interatomic distance R is given in the Methods.

Figure 3a shows the input parameters and corresponding estimated ground state energy with respect to the number of iterations at the interatomic distance of $R = 0.9$ Å. With a sufficient number of iterations, the estimated ground state energy converges to its theoretical value $E_g = -2.863$ MJ/mol. It is worth noting that the optimal eigenstate of the H-He$^+$ cation Hamiltonian at this interatomic distance is a nearly separable state, $|\psi\rangle_{\min} \sim |00\rangle$. Indeed, as shown in Fig. 3a, the input parameter H_{WM}, which determines the weak measurement strength p, converges to $H_{WM} \to \pi/4$ which means $p \to 1$.

Figure 3b presents the ground state energy as a function of the interatomic distance R. The black line represents the theoretical values, while the red circles indicate our experimental data at various interatomic distances. The minimum ground state energy of $\langle H\rangle_{\min} = -2.86 \pm 0.02$MJ/mol was obtained at the interatomic distance of $R = 0.9$ Å. The error bars represent the standard deviation calculated from the five lowest energy points during each VQE run.

To investigate the role of weak measurements, we conducted a comparative experiment without the weak measurement. For this test, we removed the weak measurement setup, the Mach-Zehnder interferometer with two PBDs, from Bob's experimental setup. The results of this modified experiment are shown as blue triangles in Fig. 3b. Details and interpretation are discussed in the Discussion.

In order to further investigate the role of pre-shared entanglement in distributed quantum computing, we tested the Schwinger Hamiltonian. This model describes the interaction between Dirac fermions via photons in a two-dimensional space[20]. The simplest form of the Schwinger Hamiltonian is presented as:

$$H(m) = 1 + XX + YY - \frac{m+1}{2}ZI + \frac{1}{2}ZZ + \frac{m}{2}IZ, \qquad (16)$$

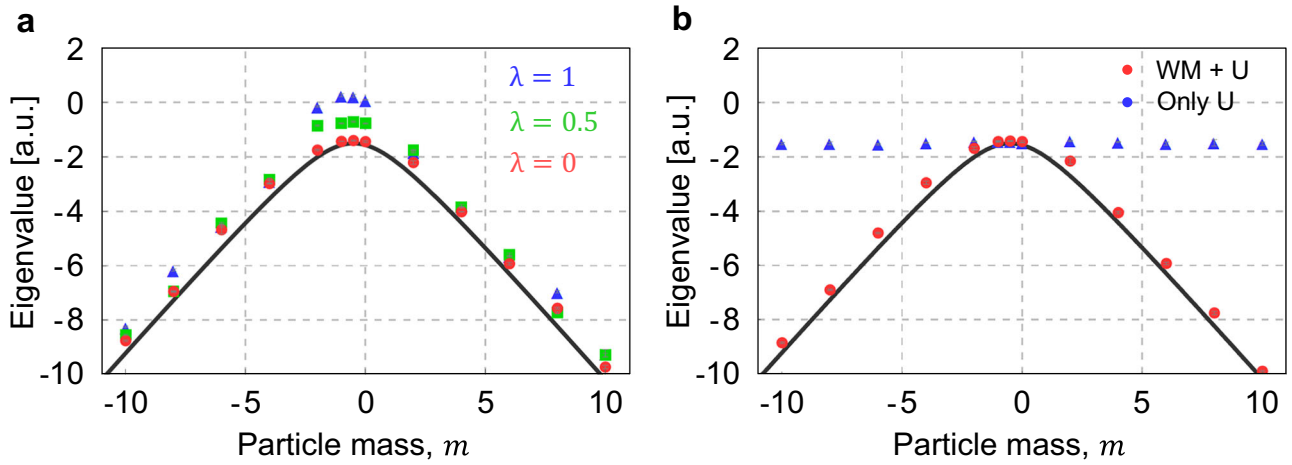

Fig. 4 | Experimental results for the evaluation of the Schwinger Hamiltonian using distributed quantum processors. a Minimum eigenvalues obtained under different strengths of dephasing noise. **b** Comparison of VQE results with and without weak measurement.

where m denotes the particle mass. The optimal eigenstate of the Schwinger Hamiltonian is computed as:

$$|\psi(m)\rangle_{\min} \sim |01\rangle - f(m)|10\rangle, \tag{17}$$

where $f(m) = \frac{1}{4}(\sqrt{4m^2 + 4m + 17} + 2m + 1)$. For $m = -1/2$, $f(m) = 1$ and the ground state becomes a maximally entangled Bell state $|\Psi^-\rangle = \frac{1}{\sqrt{2}}(|01\rangle - |10\rangle)$ with eigenvalue $E_{-1/2} = -3/2$. For other values of m, the ground state is only partially entangled.

To verify the critical role of pre-shared entanglement, we introduced variable noise to the initial state Eq. (15) by adding different lengths of quartz in Alice's quantum channel, which induce group velocity differences between $|H\rangle$ and $|V\rangle$ modes. This causes dephasing noise to the initial state, so the pre-shared state becomes:

$$\rho(\lambda) = \left(1 - \frac{\lambda}{2}\right)\sigma_{II}^{\dagger}|\Psi^+\rangle\langle\Psi^+|\sigma_{II} + \frac{\lambda}{2}\sigma_{IZ}^{\dagger}|\Psi^+\rangle\langle\Psi^+|\sigma_{IZ} \tag{18}$$

where λ represents the strength of noise. The VQE results with different amounts of noise are presented in Fig. 4a. In addition to the no-noise case (red circles for $\lambda = 0$), we present the experimental minimum eigenvalues with noise of $\lambda = 0.5$ and 1 with green squares and blue triangles, respectively. The minimal eigenvalues at $m = -1/2$ are $\langle H\rangle_{\min} = -1.40 \pm 0.02$, -0.71 ± 0.02, and 0.25 ± 0.05 for $\lambda = 0$, 0.5 and 1, respectively. It is clear that increasing noise λ introduces increasingly erroneous minimal eigenvalues near $m = -1/2$, highlighting the importance of high-fidelity pre-shared entanglement.

Furthermore, we investigated the role of weak measurements in accessing the full Hilbert space. Figure 4b shows experimental results comparing VQE implementations with and without weak measurements. Without weak measurements, the algorithm consistently converged to an eigenvalue of -1.5 regardless of m. In contrast, enabling weak measurements allowed convergence to the true ground state energies across different mass values. Further interpretation is provided in the Discussion.

Discussion

In order to clearly demonstrate the crucial role of weak measurement in the networked VQE implementation, we conducted a comparative experiment in Fig. 3b. Without weak measurement, the experimentally obtained ground state energies consistently fail to reach the theoretical values across all interatomic distances. This significant discrepancy demonstrates that without weak measurement, the system cannot access the full Hilbert space required to accurately represent the ground state of the Hamiltonian. This result confirms our theoretical prediction that weak measurement is essential for enabling distributed quantum processors to explore the complete Hilbert space necessary for effective VQE implementation.

In the case of the Schwinger Hamiltonian, the impact of noise is particularly pronounced near $m = -1/2$, where the ground state approaches a maximally entangled Bell state. In this region, the entanglement reduction caused by channel noise λ significantly degrades the VQE performance, as the algorithm cannot reach the required high entanglement level. Conversely, for larger $|m|$ values, the ground states become increasingly separable (as indicated by Eq. (17)), making them less sensitive to entanglement degradation. This explains why the error induced by noise decreases as $|m|$ increases. The results clearly demonstrate that maintaining high-fidelity pre-shared entanglement is crucial for accurately finding ground states across the entire parameter range.

Beyond entanglement quality, we also investigated the role of weak measurements in accessing the full Hilbert space. In our experimental setup with an initially shared maximally entangled Bell state, reaching the ground state when $m = -1/2$ requires only local unitary operations since these preserve the entanglement level. However, for $m \neq -1/2$, where the ground state is partially entangled, weak measurements become necessary to reduce the entanglement to the appropriate level. Figure 4b demonstrates this critical distinction. When employing VQE without weak measurements and starting from a maximally entangled state, the algorithm consistently converges to an eigenvalue of -1.5, indicating the final state remains maximally entangled (the $|\Psi^-\rangle$ state). This occurs regardless of the target mass parameter, as the procedure lacks a mechanism to reduce entanglement to reach partially entangled ground states for $m \neq -1/2$.

In contrast, with weak measurements enabled, our procedure successfully converges to the true ground state energy across various mass values. These results collectively demonstrate that both high-quality pre-shared entanglement and the ability to manipulate entanglement through weak measurements are essential for effective distributed quantum computing. This combination provides the flexibility needed to access states with different entanglement levels based on specific problem requirements.

In conclusion, we have successfully implemented a distributed variational quantum eigensolver using photonic quantum processors connected through a 3 km optical fiber network. Our approach introduces a fundamentally different paradigm for distributed quantum computing by integrating parameterized weak measurements with local unitary operations to achieve precise control over pre-shared entanglement. This combination provides full access to the two-qubit Hilbert space without requiring complex non-local operations that are typically necessary in distributed architectures.

Table 1 | The Pauli operators and corresponding weights that form the Hamiltonian, shown in relation to the interatomic distance

R [Å]	II	IZ	ZI	ZZ	IX	ZX	XI	XZ	XX
0.05	33.9557	−2.4784	−2.4784	0.2746	−0.1515	0.1515	−0.1515	0.1515	0.1412
0.1	13.3605	−2.4368	−2.4368	0.2081	−0.1626	0.1626	−0.1626	0.1626	0.2097
0.2	3.633	−2.2899	−2.2899	0.1176	−0.1405	0.1405	−0.1405	0.1405	0.3027
0.5	−2.3275	−1.5236	−1.5236	0.1115	−0.157	0.157	−0.157	0.157	0.3309
0.7	−3.3893	−1.2073	−1.2073	0.1626	−0.1968	0.1968	−0.1968	0.1968	0.3052
0.9	−3.8505	−1.0466	−1.0466	0.2356	−0.2288	0.2288	−0.2288	0.2288	0.2613
1.1	−4.0539	−0.982	−0.982	0.3225	−0.243	0.243	−0.243	0.243	0.2053
1.5	−4.1594	−0.991	−0.991	0.4945	−0.2086	0.2086	−0.2086	0.2086	0.0948
2	−4.1347	−1.0605	−1.0605	0.6342	−0.1119	0.1119	−0.1119	0.1119	0.0212
2.5	−4.0918	−1.1128	−1.1128	0.701	−0.0454	0.0454	−0.0454	0.0454	0.0032

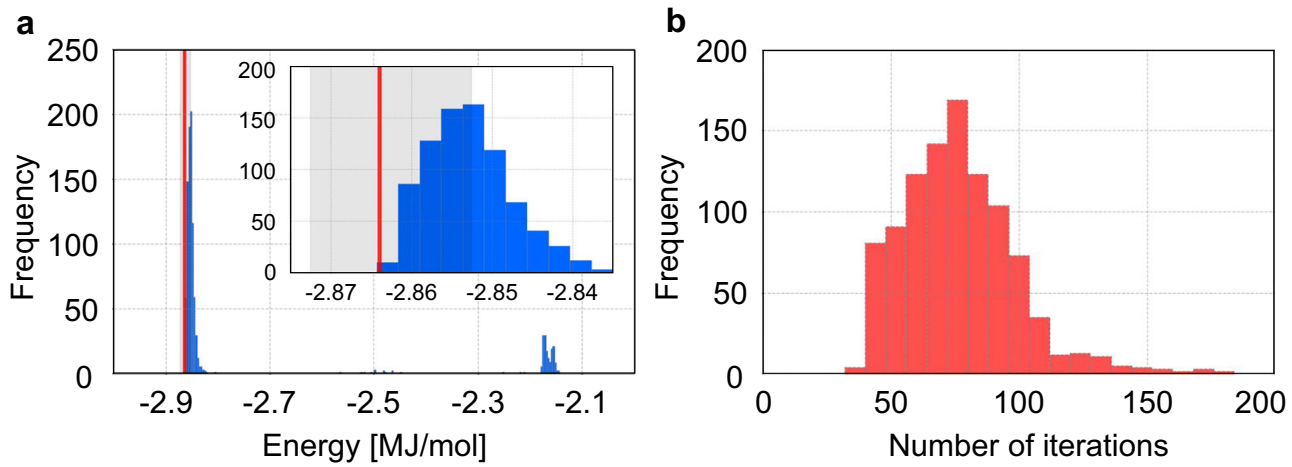

Fig. 5 | The classical computer emulation test results of the classical optimizers with 1000 trials. a The estimated energy (**b**) the number of iterations. In **a** the red solid line represents theoretical value of our simulated Hamiltonian, $E_g = -2.863$ MJ/mol. The gray region shows the optimizer's convergence tolerance $tol = 0.01$, which corresponds to the convergence criterion.

Notably, our scheme maintains favorable resource scaling with only $\mathcal{O}(n)$ additional weak measurement parameters-one per Bell pair-complementing the $\mathcal{O}(n)$ to $\mathcal{O}(n^2)$ variational parameters required by typical VQE ansatz. This linear overhead avoids the complexity of gate teleportation, which requires additional Bell pairs and classical communication for each non-local gate, with overhead scaling with circuit depth rather than system size alone. Leveraging pre-shared entanglement and using weak measurements to tune the amount of entanglement, our approach offers a resource-efficient framework for scaling quantum networks with multiple Bell pairs between nodes.

Through evaluations of both the H-He$^+$ cation Hamiltonian and the Schwinger model, we have demonstrated that weak measurements play a crucial role in distributed quantum computation. Our experimental results clearly show that without weak measurement capabilities, the quantum processors cannot access states with the appropriate entanglement structure required to represent ground states of general Hamiltonians. Additionally, we verified that high-quality pre-shared entanglement is essential, as degradation in entanglement fidelity directly impacts solution accuracy.

Our demonstration highlights the versatility of photonic qubits not only as carriers of quantum information across networks but also as capable processing elements for quantum computation. The success of our weak measurement-assisted distributed quantum computing approach establishes a viable and adaptable framework for future quantum information processing technologies that harness the power of quantum networks[42].

Methods

H-He$^+$ cation Hamiltonian

In the framework of second-order quantization, any Hamiltonian can be expressed as

$$H = \sum_{p,q} h_{p,q} a_p^\dagger a_q + \sum_{p,q,r,s} h_{p,q,r,s} a_p^\dagger a_q^\dagger a_r a_s + \cdots, \tag{19}$$

where $a^\dagger$ and a denote the creation and annihilation operators, respectively. Through the Jordan-Wigner transformation, equation (19) can be reformulated as a linear sum of Pauli operators: (19) an be presented as a linear summations of Pauli operators as

$$H = \sum_j w_j \cdot \boldsymbol{\sigma}_j + \sum_{jk} w_{jk} \cdot \boldsymbol{\sigma}_j \otimes \boldsymbol{\sigma}_k + \cdots. \tag{20}$$

The coefficients w_j, w_{jk}, $\cdots$ are calculated during the transformation. The coefficients are presented in Table 1. Here, X, Y, Z, I correspond to the Pauli matrices σ_x, σ_y, σ_z and the identity operators, respectively[14].

The classical optimizer

We evaluated the hyperparameters of the COBYLA optimizer using 1000 emulation runs on a classical computer. The initial parameters were randomized for each run, and we accounted for a Bell state purity of 0.98 and used 50,000 shots to reflect the experimental conditions. Figure 5a shows the histogram of the estimated energy, and Fig. 5b shows the number of

iterations. In Fig. 5a, the red vertical line indicates the theoretical value $E_g = -2.863$ MJ/mol. The gray region represents the convergence tolerance range of the optimizer, $tol = 0.01$. The mean estimated energy value is -2.853 ± 0.006 MJ/mol, which differs negligibly from the theoretical value and is mainly due the Bell state purity. From Fig. 5b, the mean number of iterations is 76, indicating that a maximum iteration cap of 200 is sufficient.

Data availability

The data and analysis scripts are available from the corresponding author upon reasonable request.

Code availability

We cite the specific COBYLA implementation used in this study[41]. Supporting scripts used in the analysis (including hyperparameter settings and emulation routines) are available upon reasonable request.

Received: 31 July 2025; Accepted: 10 December 2025;
Published online: 03 January 2026

References

1. Preskill, J. Quantum computing in the NISQ era and beyond. *Quantum* **2**, 79 (2018).
2. Chae, E., Choi, J. & Kim, J. An elementary review on basic principles and developments of qubits for quantum computing. *Nano Convergence* **11**, 11 (2024).
3. Grover, L. K. Quantum telecomputation. Preprint at https://doi.org/10.48550/arXiv.quant-ph/9704012 (1997).
4. Cirac, J. I., Ekert, A. K., Huelga, S. F. & Macchiavello, C. Distributed quantum computation over noisy channels. *Phys. Rev. A* **59**, 4249 (1999).
5. Jiang, L., Taylor, J. M., Sørensen, A. S. & Lukin, M. D. Distributed quantum computation based on small quantum registers. *Phys. Rev. A* **76**, 062323 (2007).
6. Caleffi, M. et al. Distributed quantum computing: a survey. *Comp. Net.* **254**, 110672 (2024).
7. Pirandola, S., Eisert, J., Weedbrook, C., Furusawa, A. & Braunstein, S. L. Advances in quantum teleportation. *Nat. Photon.* **9**, 641 (2015).
8. Daiss, S. et al. A quantum-logic gate between distant quantum-network modules. *Science* **371**, 614 (2021).
9. Liu, X. et al. Nonlocal photonic quantum gates over 7.0 km. *Nat. Commun.* **15**, 8529 (2024).
10. Lai, P.-C. et al. Realization of a crosstalk-free two-ion node for long-distance quantum networking. *Phys. Rev. Lett.* **134**, 070801 (2025).
11. Kim, Y.-S., Cho, Y.-W., Ra, Y.-S. & Kim, Y.-H. Reversing the weak quantum measurement for a photonic qubit. *Opt. Express* **17**, 11978 (2009).
12. Xu, X.-Y., Xu, J.-S., Li, C.-F., Zou, Y. & Guo, G.-C. Experimental demonstration of nonlocal effects in the partial-collapse measurement and reversal process. *Phys. Rev. A* **83**, 010101(R) (2011).
13. Kim, Y.-S., Lee, J.-C., Kwon, O. & Kim, Y.-H. Protecting entanglement from decoherence using weak measurement and quantum measurement reversal. *Nat. Phys.* **8**, 117 (2012).
14. Peruzzo, A. et al. A variational eigenvalue solver on a photonic quantum processor. *Nat. Commun.* **5**, 1 (2014).
15. McClean, J. R., Romero, J., Babbush, R. & Aspuru-Guzik, A. The theory of variational hybrid quantum-classical algorithms. *N. J. Phys.* **18**, 023023 (2016).
16. Bharti, K. et al. Noisy intermediate-scale quantum algorithms. *Rev. Mod. Phys.* **94**, 015004 (2022).
17. O'Malley, P. J. J. et al. Scalable quantum simulation of molecular energies. *Phys. Rev. X* **6**, 031007 (2016).
18. Kandala, A. et al. Hardware-efficient variational quantum eigen-solver for small molecules and quantum magnets. *Nature* **549**, 242–246 (2017).
19. Kokail, C. et al. Self-verifying variational quantum simulation of lattice models. *Nature* **569**, 355–360 (2019).
20. Borzenkova, O. V. et al. Variational simulation of Schwinger's Hamiltonian with polarization qubits. *Appl. Phys. Lett.* **118**, 144002 (2021).
21. Lee, D. et al. Error-mitigated photonic variational quantum eigensolver using a single-photon ququart. *Optica* **9**, 88 (2022).
22. Zhao, L. et al. Orbital-optimized pair-correlated electron simulations on trapped-ion quantum computers. *npj Quantum Inf.* **9**, 60 (2023).
23. Lee, J. et al. Photonic variational quantum eigensolver using entanglement measurements. *Quantum Sci. Technol.* **9**, 045028 (2024).
24. Kim, B. et al. Qudit-based variational quantum eigensolver using photonic orbital angular momentum states. *Sci. Adv.* **10**, eado3472 (2024).
25. Hwang, K., Lim, H.-T., Kim, Y.-S., Park, D. K. & Kim, Y. Distributed quantum machine learning via classical communication. *Quantum Sci. Technol.* **10**, 015059 (2024).
26. Main, D. et al. Distributed quantum computing across an optical network link. *Nature* **638**, 383 (2025).
27. Nielsen, M. A. & Chuang, I. L.*Quantum Computation and Quantum Information* (Cambridge Univ. Press, 2010).
28. Nielsen, M. Conditions for a class of entanglement transformations. *Phys. Rev. Lett.* **83**, 436 (1999).
29. Horodecki, R., Horodecki, P., Horodecki, M., Horodecki, K. & Goyeneche, D. Quantum entanglement. *Rev. Mod. Phys.* **81**, 865 (2009).
30. Vaidman, L. Instantaneous measurement of nonlocal variables. *Phys. Rev. Lett.* **90**, 010402 (2003).
31. Dür, W., Vidal, G. & Cirac, J. I. Three qubits can be entangled in two inequivalent ways. *Phys. Rev. A* **62**, 062314 (2000).
32. Bennett, C. H., Popescu, S., Rohrlich, D., Smolin, J. A. & Thapliyal, A. V. Exact and asymptotic measures of multipartite pure-state entanglement. *Phys. Rev. A* **63**, 012307 (2000).
33. Brodutch, A. & Cohen, E. Nonlocal measurements via quantum erasure. *Phys. Rev. Lett.* **116**, 070404 (2016).
34. Li, Y. et al. Experimental nonlocal measurement of a product observable. *Optica* **6**, 1199 (2019).
35. Kim, T., Fiorentino, M. & Wong, F. N. C. Phase-stable source of polarization-entangled photons using a polarization sagnac interferometer. *Phys. Rev. A* **73**, 012316 (2006).
36. Hong, S. et al. Quantum enhanced multiple-phase estimation with multi-mode n00n states. *Nat. Commun.* **12**, 5211 (2021).
37. Kim, D.-H. et al. Distributed quantum sensing of multiple phases with fewer photons. *Nat. Commun.* **15**, 266 (2024).
38. Yoon, J. et al. Experimental comparison of various quantum key distribution protocols under reference frame rotation and fluctuation. *Opt. Commun.* **441**, 64 (2019).
39. Park, B. K., Kim, Y.-S., Kwon, O., Han, S.-W. & Moon, S. High-performance reconfigurable coincidence counting unit based on a field programmable gate array. *Appl. Opt.* **54**, 4727 (2015).
40. Park, B. K., Kim, Y.-S., Cho, Y.-W., Moon, S. & Han, S.-W. Arbitrary configurable 20-channel coincidence counting unit for multi-qubit quantum experiment. *Electronics* **10**, 569 (2021).
41. SciPy Developers. minimize(method=cobyla) — scipy manual (2023). https://docs.scipy.org/doc/scipy-1.11.1/reference/optimize.minimize-cobyla.html. Version used: v1.11.1 (June 28, 2023); Accessed: 2025-10-01.
42. Wehner, S., Elkouss, D. & Hanson, R. Quantum internet: a vision for the road ahead. *Science* **362**, eaam9288 (2018).

Acknowledgements

The authors acknowledged the support by National Information Society Agency(NIA) funded by the Ministry of Science and ICT(MSIT, Korea) [Quantum technology test verification and consulting support in

2024]. National Research Foundation of Korea (RS-2023-NR119925, RS-2024-00509800); Korea Institute of Science and Technology (2E33541).

Author contributions

D.L. and Y.-S.K. wrote the main manuscript text and prepared the figures. They also designed and performed the experiment and analyzed the data. J.L. contributed to the theoretical analysis and the Theory section. B.B. contributed to the Methods section and the experimental implementation. Y.K., S.-W.L., and H.-T.L. provided feedback and critical comments. All authors reviewed the manuscript.

Competing interests

The authors declare no competing interests.

Additional information

Correspondence and requests for materials should be addressed to Yong-Su Kim.

Reprints and permissions information is available at http://www.nature.com/reprints

Publisher's note Springer Nature remains neutral with regard to jurisdictional claims in published maps and institutional affiliations.